Thermodynamic Instabilities in One Dimension: Correlations, Scaling and Solitons

Thierry Dauxois, Nikos Theodorakopoulos, Michel Peyrard

Thermodynamic instabilities in one dimension: correlations, scaling and solitons

Thierry Dauxois[1], Nikos Theodorakopoulos[2] and Michel Peyrard[1]
[1] *Laboratoire de Physique, UMR-CNRS 5672, ENS Lyon, 46 Allée d'Italie, 69007 Lyon, France*
[2] *Theoretical and Physical Chemistry Institute, National Hellenic Research Foundation, Vasileos Constantinou 48, 116 35 Athens, Greece*
(Dated: April 12, 2015)

Many thermodynamic instabilities in one dimension (e.g. DNA thermal denaturation, wetting of interfaces) can be described in terms of simple models involving harmonic coupling between nearest neighbors and an asymmetric on-site potential with a repulsive core, a stable minimum and a flat top. The paper deals with the case of the Morse on-site potential, which can be treated exactly in the continuum limit. Analytical expressions for correlation functions are derived; they are shown to obey scaling; numerical transfer-integral values obtained for a discrete version of the model exhibit the same critical behavior. Furthermore, it is shown in detail that the onset of the transition can be characterized by an entropic stabilization of an -otherwise unstable-, nonlinear field configuration, a soliton-like domain wall (DW) with macroscopic energy content. The statistical mechanics of the DW provides an exact estimate of the critical temperature for a wide range of the discretization parameter; this suggests that the transition can be accurately viewed as being "driven" by a nonlinear entity.

I. INTRODUCTION

In a seminal paper published a quarter-century ago, Krumhansl and Schrieffer [1] explored the possibility that nonlinear excitations (solitons) might drive structural phase transitions. They succeeded in identifying signatures of "domain walls (DW)" in the thermodynamic properties of the one-dimensional ϕ^4 model and gave a phenomenological account of a salient feature of structural phase transitions, the appearance of a central peak in the dynamical spectrum. However, important issues remained open. In particular, because the demonstration was limited to a system which does not exhibit a genuine (i.e. finite-temperature) thermodynamic phase transition, there was no possibility to explore the role of exact, or nearly exact, nonlinear field configurations in determining critical behavior, static or dynamic.

A class of one-dimensional models, which has been proposed to describe a wide variety of thermodynamic instabilities, such as thermal DNA denaturation [2–4], wetting of interfaces [5], and other similar phenomena, could prove to be of interest in the above context. Typically, such models include a short-range interaction between near neighbors, and an on-site potential with a single minimum and a flat-top; in the context of DNA denaturation, as the temperature increases, particles begin to access the region of the flat top at an increasing rate, until, at a finite temperature, a macroscopic instability occurs, with a divergence in the average displacement (the "effective length" of the hydrogen bond which holds the double-stranded chain together), a divergent correlation length, and, generally, all the characteristics of a thermodynamic phase transition. In the simplest case, that of a harmonic interaction and a Morse on-site potential, the thermodynamics can be calculated exactly by using functional integral techniques [1] and mapping the problem to the quantum mechanics of the Morse oscillator. The thermodynamic transition corresponds to the quantum mechanics of the disappearance of the last bound state.

In this paper, we will show that soliton physics can offer a correct interpretation of such thermodynamic instabilities. In particular, a relatively brief calculation can show us *why* and *when* a thermodynamic transition occurs. The logic can be summarized as follows: An exact, static nonlinear configuration of the continuum field can be found, which "interpolates" between the low- and the high-temperature phase. We interpret this to a be a DW. The total energy of the configuration diverges, because each site which is in the high-temperature phase contributes a finite amount of bond (and elastic) energy. The infinity is in a sense a "minimal requirement": as long as the DW energy is finite, no phase transition can occur in one dimension [6]. A closer look at the properties of the DW is more revealing. In contrast to other Klein-Gordon field theories with a finite-energy kink, there is no zero-frequency Goldstone mode. It costs energy to shift the position of DW so that it can include more sites at the high-temperature phase. Conversely, there is an energy gain by "zipping back" to the low-temperature phase. At finite temperatures, the picture must be corrected to include entropic effects. The "phonon cloud" which accompanies the DW provides an entropic gain which ultimately balances the energy cost of extending the DW to macroscopic scale. The formation of a thermally stable DW is thus seen to "drive" the instability. At higher temperatures, it is entropically advantageous for a DW to extend itself by "unzipping" more sites towards the high temperature phase. The picture sketched above, which concentrates entirely on the thermal stability of the nonlinear interface, is more than a qualitative nonlinear scenario. It provides an estimate of the transition temperature which (i) turns out to be exact within the continuum field framework and, (ii) can be *nonperturbatively* extended to describe lattice systems up to quite high levels of discretization.

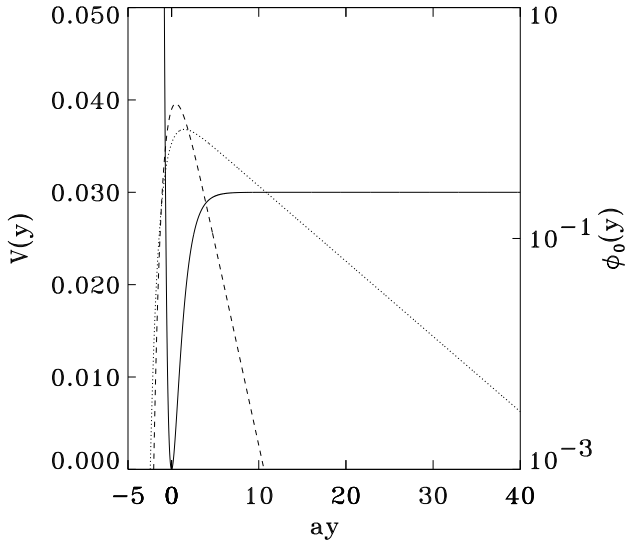

FIG. 1: The Morse potential $V(y)$ is shown (solid line) as a function of the dimensionless field ay. The groundstate wavefunction $\phi_0(y)$ (Eq. (2.19)) is shown for different values of the temperature: dashed line for $T = T_c/2.6$, dotted line for $T = T_c/1.3$. Note the logarithmic scale for $\phi_0(y)$.

The paper is structured as follows: Section II provides a full account of exact results for the model. This is important to establish notation and context for the discussion. Moreover, although some results have appeared in the literature before, they are scattered in various sources; in addition, results for the correlation function and the susceptibility are new and the calculation has not been reported elsewhere [7]. Section III deals with the soliton physics of the transition. A brief discussion of results and further perspectives, with special emphasis to effects due to lattice discreteness, is given in Section IV.

II. EXACT THERMODYNAMICS

A. Model and notation

The Hamiltonian of the model is [3]

$$H = \sum_n \left[\frac{p_n^2}{2m} + \frac{K}{2}(y_n - y_{n-1})^2 + V(y_n) + Dhay_n \right] \tag{2.1}$$

where m is the reduced mass of a base pair, y_n denotes the stretching of the hydrogen bonds connecting the two bases of the n^{th} pair and $p_n = m(dy_n/dt)$ corresponds to the conjugate momentum of y_n.

In addition to the kinetic and nearest-neighbor potential energy terms, (2.1) contains: (i) an on-site potential which describes the interaction of the two bases in a pair; the Morse potential

$$V(y_n) = D\ (e^{-ay_n} - 1)^2 \quad , \tag{2.2}$$

plotted in Fig. 1, has been chosen because it has the correct qualitative shape; and (ii), a field-dependent term, which describes the effect of a transverse, external stress h.

A set of parameters which has been used in the DNA denaturation context [3, 4] is: a dissociation energy $D = 0.03$ eV, a coupling constant $K = 0.06$ eV/Å^2, a spatial scale factor of the Morse potential $a = 4.5$ Å^{-1}, and a mass $m = 300$ a.m.u; the time scale is determined by $\omega_0 = (K/m)^{1/2}$. The dimensionless ratio $R = Da^2/K$ is traditionally used to distinguish between the "order-disorder" (discrete, $R \gg 1$) and "displacive" (continuum, $R \ll 1$) regime; the given set of parameters corresponds to $R = 10.1$.

The classical thermodynamic properties of (2.1) can be described exactly in terms of the transfer integral (TI) equation [1, 8]

$$\int_{-\infty}^{+\infty} dy\ e^{-\beta[V(x)+V(y)+2W(x,y)+Dah(y+x)]/2}\ \phi_n(y) = e^{-\beta\varepsilon_n}\ \phi_n(x) \quad , \tag{2.3}$$

where $\beta = 1/(k_B T)$, k_B is the Boltzmann constant and T is the temperature.

In general, we are interested in situations for which $h = 0$; however, the external field is useful in practical calculations as a mathematical device. For example, by letting $h \to 0^+$ it is possible to extract the scaling behavior near the transition; moreover, since the partition function is now divergence-free at any $h > 0$ (and numerical calculations can in principle be performed at finite, decreasing h), previous criticism of the model on formal mathematical grounds [9] is addressed.

In the thermodynamic limit, the free energy per site (except for a nonsingular term due to the integral over momenta) is determined by the smallest eigenvalue ε_0 of (2.3), i.e.,

$$f = \varepsilon_0 - \frac{1}{2\beta} \ln \left[\frac{2\pi m}{\beta} \right] \tag{2.4}$$

Other thermodynamic properties of interest are (i) the order parameter

$$\sigma = < y > = \int_{-\infty}^{+\infty} dy \; y \; |\phi_0|^2 \tag{2.5}$$

where ϕ_0 is the normalized eigenstate corresponding to the eigenvalue ε_0 and (ii) the correlation function

$$C(j) \equiv < (y_j - \sigma)(y_0 - \sigma) > \; = \sum_{n=1}^{+\infty} |M_n|^2 e^{-\Delta_n |j|}, \tag{2.6}$$

where the sum runs over states other than ϕ_0,

$$\Delta_n \equiv \beta(\varepsilon_n - \varepsilon_0) \quad , \tag{2.7}$$

and the off-diagonal matrix elements M_n are given (in Dirac notation) by

$$M_n = < n|(y - < y >)|0 > = < n|y|0 > \quad . \tag{2.8}$$

B. The corresponding Morse oscillator problem

In the gradient expansion (continuum) approximation,

$$\phi_n(y) = \phi_n(x) + \phi_n'(x)(y - x) + \phi_n''(x)(y - x)^2/2 + \mathcal{O}\left((y - x)^3\right) \quad , \tag{2.9}$$

which is strictly valid in the temperature window $D \ll k_B T \ll D/R$ [10], the integral equation (2.3) can be well approximated by the second-order differential equation

$$\left[-\frac{1}{2\beta^2 K} \frac{d^2}{dy^2} + D(e^{-ay} - 1)^2 + Dhay \right] \phi_n(y) = e_n \; \phi_n(y) \quad . \tag{2.10}$$

where $e_n = \varepsilon_n + \ln(2\pi/\beta K)/2\beta$. The one-dimensional statistical mechanics TI problem is thus mapped [2] to the zero-dimensional quantum mechanics problem of the Morse oscillator.

In the following, we will list and/or derive some general properties of (2.12) at $h = 0$. The change of variables

$$z = 2\delta \exp(-ay) \quad \text{with} \quad \delta = \frac{\beta}{a} \sqrt{2DK} \quad , \tag{2.11}$$

the transformation $\phi_n(y) = e^{-z/2} \; z^s \; w_n(z)$ and $s = \delta \sqrt{1 - e_n/D}$, leads to

$$z \frac{d^2 w_n}{dz^2} + (2s + 1 - z) \frac{dw_n}{dz} + n w_n = 0 \quad , \tag{2.12}$$

where $n = \delta - s - 1/2$. If n is a positive integer, the solution of (2.12) is a Laguerre polynomial [11].

C. Bound state(s) and associated distinct length scales

Noting that $\phi_n(y)$ remains finite over the interval $[0, +\infty[$ only for positive values of s, we obtain the spectrum of bound states,

$$\frac{e_n}{D} = 1 - \left(1 - \frac{n+1/2}{\delta}\right)^2 \quad \text{with} \quad n = 0, 1, \ldots, E(\delta - 1/2)\ , \tag{2.13}$$

where $E(\delta - 1/2)$ is the integer part of $\delta - 1/2$. It follows that as long as δ exceeds a critical value $\delta_c = 1/2$, the ground state remains bounded. In the quantum problem, this provides a criterion for the critical mass of a particle below which it is driven out of the potential well by quantum fluctuations. We note that this is a general property of asymmetric potential wells; symmetric wells support a bound state for any value of δ [18, 19].

Using (2.11), this δ_c defines a critical temperature

$$T_c = \frac{2\sqrt{2KD}}{ak_B} \tag{2.14}$$

in terms of which $\delta = T_c/2T$. As the temperature approaches T_c, the last bound state becomes less and less localized, and $< y >$ increases sharply, indicating the "melting" of the system.

Using (2.4) results in a free energy per site $f = e_0 + f_0$, where

$$f_0 = -\frac{1}{\beta} \ln\left(\frac{2\pi}{\beta\omega_0}\right) \tag{2.15}$$

and

$$\begin{aligned} e_0 &= D\left[1 - |t|^2\right] \qquad \text{if } T < T_c \\ &= D \quad \text{otherwise} \end{aligned} \tag{2.16}$$

where $t = T/T_c - 1$ is the reduced temperature; it follows that the entropy per site can be written as the sum of a non-singular part

$$S_{non-sing} = S(T_c) + k_B \log\left(\frac{T}{T_c}\right) \tag{2.17}$$

and a singular part,

$$\begin{aligned} S_{sing} &= \frac{2D}{T_c}\, t \qquad \text{if} \qquad T < T_c \\ &= 0 \qquad\qquad \text{otherwise.} \end{aligned} \tag{2.18}$$

We note that (2.18) implies a jump discontinuity of the specific heat at T_c; this is consistent with a specific heat critical exponent $\alpha = 0$.

For $T_c/3 < T < T_c$, the (normalized) ground state

$$\phi_0 = \sqrt{\frac{a}{\Gamma(2\delta - 1)}}\ e^{-z/2}\ z^{\delta - 1/2}\ , \tag{2.19}$$

where Γ is the gamma function, is the only bound state. The asymptotic behavior $\phi_0(y) \propto e^{-a(\delta-1/2)y}$ defines the spatial extent of the ground state

$$\lambda = \frac{1}{a(\delta - 1/2)} \quad . \tag{2.20}$$

The order parameter, obtained from Eqs. (2.5) and (2.19), is [12]

$$\sigma = \frac{1}{a}\left[\ln(2\delta) - \psi(2\delta - 1)\right] \tag{2.21}$$

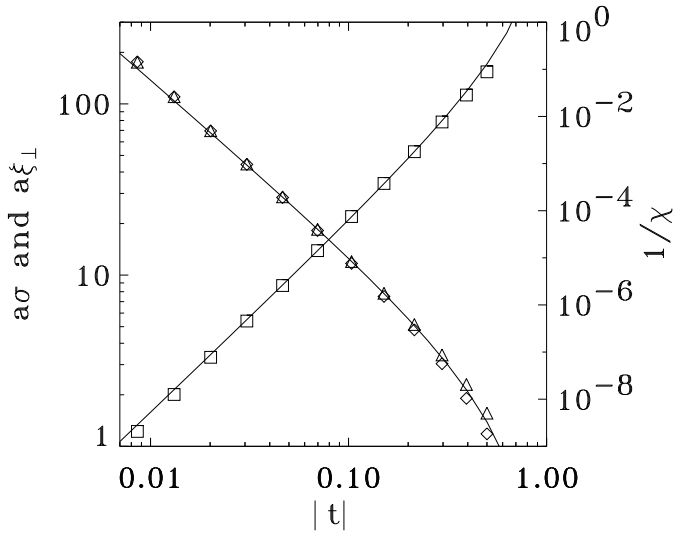

FIG. 2: Left scale: dependence of the order parameter σ (diamonds) and its fluctuations $\xi_\perp$ (triangles) as a function of the reduced temperature t; the points were obtained numerically using the TI method; the solid line shows the analytical estimate, Eq. (2.22), with $\delta_c = 0.36$. Right scale: the susceptibility χ as a function t (squares: numerical TI; solid line: Eq. (2.40) with $\delta_c = 0.36$).

where ψ is the digamma function; in the vicinity of the critical temperature, this reduces to

$$\sigma \sim \frac{1}{a(2\delta - 1)} = \frac{\lambda}{2} = \frac{1}{2a\delta_c} \frac{T}{T_c} |t|^{-1} \quad ; \tag{2.22}$$

in the language of phase transitions, $\sigma \propto |t|^\beta$, where $\beta = -1$ is the critical exponent for the order parameter, i.e. the order parameter *diverges* at the instability. Fig. 2 shows that the agreement of numerical TI values with (2.22) is excellent, provided one takes into account the numerical TI value of $\delta_c = 0.36$ (corresponding to $T_c = 427K$) for the discrete system.

Local fluctuations of the order parameter are described by [12]

$$\xi_\perp = \sqrt{< 0 \mid (y - \sigma)^2 \mid 0 >} = \frac{\sqrt{\psi' (2\delta - 1)}}{a} \quad . \tag{2.23}$$

In the vicinity of the critical temperature, this reduces to

$$\xi_\perp \sim \frac{1}{a(2\delta - 1)} = \frac{\lambda}{2} \tag{2.24}$$

which implies $\xi_\perp \propto |t|^{-\nu_\perp}$ with $\nu_\perp = -\beta = 1$. Close to the transition, the order parameter and its fluctuations are therefore comparable, as shown by Fig. 2; in the wetting literature [5] they are both interchangeably referred to as "transverse correlation lengths".

If we denote the lattice constant by ℓ and identify the next-to-lowest eigenstate with the bottom of the continuum band, we obtain the inverse longitudinal correlation length

$$\frac{\ell}{\xi_{||}} = \beta(e_1 - e_0) \simeq \beta(D - e_0) = \beta D \ |t|^2 = \frac{\beta D}{(\delta a \lambda)^2} \tag{2.25}$$

i.e. the corresponding critical exponent $\nu_{||} = 2$. The solid line plotted in Fig. (3) shows a perfect agreement for the difference of the two first eigenvalues, between Eq. (2.25) and numerical TI results.

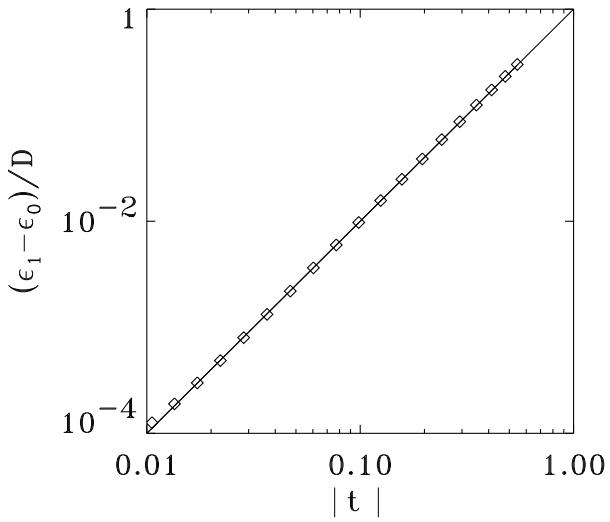

FIG. 3: Dependence of $(e_1 - e_0)/D$ on the reduced temperature. The solid line corresponds to the exact (continuum) result $|t|^2$, cf. (2.25). The diamonds are numerical TI results.

D. Static structure factor and susceptibility

In terms of the correlation functions derived above, the static structure factor reads

$$S(q,T) = \sum_{j=-\infty}^{+\infty} e^{iqj\ell}\, C(j) \tag{2.26}$$

$$= \sum_{j=-\infty}^{+\infty}\sum_{\kappa=1}^{+\infty} |M_\kappa|^2 e^{iqj\ell-\Delta_\kappa|j|} \tag{2.27}$$

$$= \sum_{\kappa=1}^{+\infty} |M_\kappa|^2 \frac{\sinh\Delta_\kappa}{\cosh\Delta_\kappa - \cos(q\ell)}\ , \tag{2.28}$$

where the sum extends over all the scattering states of Eq. (2.10). They are given by the second solution [13] of the confluent hypergeometric equation (2.12) for imaginary $s = i\kappa$. In the notation of Eq. (13.1.1) of Ref. [13], the solution $w(z) = U(1/2 - \delta + i\kappa, 1 + 2i\kappa, z)$ has the correct asymptotic behavior: it grows as $z^{\delta-1/2-i\kappa}$ as $z \to +\infty$ (i.e., $y \to -\infty$), so that the exponential prefactor in the definition of ϕ_κ dominates the vanishing of the wavefunction at the Morse hard core. These scattering states correspond to plane wave superposition

$$w(z) \propto 1 - e^{2i\theta(\kappa,\delta)} z^{-2i\kappa} \tag{2.29}$$

as $z \to 0$ (i.e., $y \to +\infty$) where $\theta(\kappa) = \arg\Gamma(1 + 2i\kappa) + \arg\Gamma(1/2 - \delta - i\kappa)$. The unnormalized continuum eigenstates are therefore given in the asymptotic limit $y \to \infty$ by

$$\phi_\kappa(y) = \sin(\kappa a y + \theta(\kappa)) \tag{2.30}$$

and the corresponding eigenvalues by

$$e_\kappa = D\left(1 + \kappa^2/\delta^2\right) \quad . \tag{2.31}$$

As ε_κ and e_κ differ by a quantity that does not depend on κ, from (2.31) and (2.7) we identify

$$\Delta_\kappa = \frac{\beta D}{\delta^2}\left[(\delta - 1/2)^2 + \kappa^2\right] \quad . \tag{2.32}$$

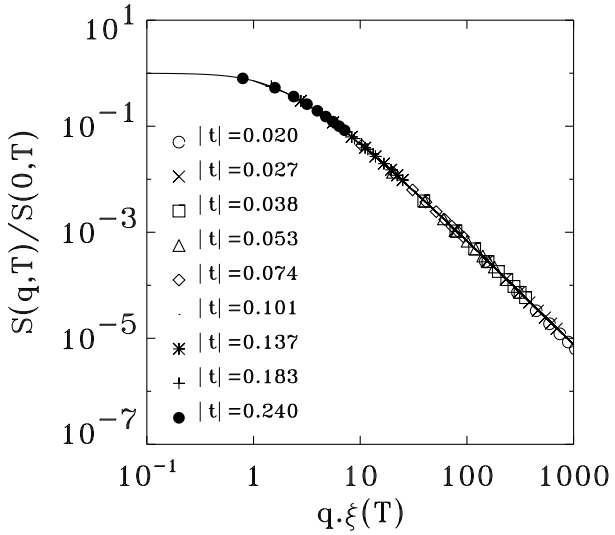

FIG. 4: The reduced static structure factor $S(q,T)/S(0,T)$ as a function of $q\xi$ for different values of the reduced temperature.The solid line is the theoretical curve (2.39) whereas the symbols were obtained using the TI method for different values of the temperature.

Near the critical instability and in the long-wavelength limit $q\ell \ll 1$, the static structure factor can be calculated as follows for a given value of $q\xi_{||}$. Due to the rapid oscillations of the scattering eigenstates (2.30), matrix elements will vanish for large values of κ whereas, for small κ, the phase shift can be approximated by $\theta = -\arctan(\kappa\lambda a)$. Since the ground state extends to large values of y, for most of the interval of integration we can use the asymptotic form (2.30) of the continuum states. Normalizing in a box of size $(\mathcal{O}(L^0), L/2)$ to account for the soft core, the ground and excited states are respectively

$$\phi_0(y) \simeq \sqrt{\frac{2}{\lambda}} e^{-y/\lambda} \tag{2.33}$$

$$\phi_\kappa(y) \simeq \frac{2i}{\sqrt{L}} \sin(\kappa a y + \theta(\kappa)), \tag{2.34}$$

where L is the system size. We obtain

$$M_\kappa \simeq i\sqrt{\frac{8\lambda^3}{L}} \frac{\sin(\sigma+\theta)}{1+\kappa^2\lambda^2 a^2} \tag{2.35}$$

where $\sigma \equiv 2\arctan(\kappa\lambda a) = -2\theta$. This explicitly gives $\tan(\theta+\sigma) = \kappa\lambda a$ and hence

$$|M_\kappa|^2 \simeq \frac{8\lambda^3}{L} \frac{\kappa^2\lambda^2 a^2}{(1+\kappa^2\lambda^2 a^2)^3} \, . \tag{2.36}$$

In order to substitute the sum over κ by an integral in Eq. (2.28), we need the correct density of space in κ space; this can be obtained by setting the eigenfunction of (2.34) equal to zero at the boundary $x = L/2$ and leads to a density of states $aL/2\pi$. Eq. (2.28) can be rewritten as

$$S(q,T) = \lambda^2 \frac{\xi_{||}}{\ell} F(q\xi_{||}) \quad , \tag{2.37}$$

where

$$F(x) = \frac{2}{x^2}\left[1 - \frac{1}{\cosh(\mathrm{arcsinh}(x)/2)}\right] \quad . \tag{2.38}$$

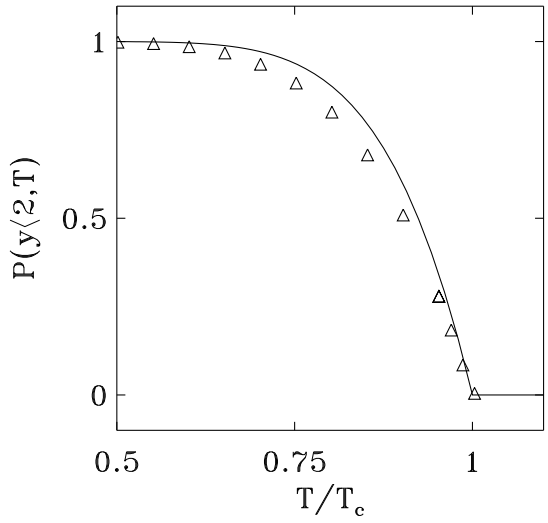

FIG. 5: The fraction of bound base pairs $P(y < 2\mathring{A}, T)$ as a function of the T/T_c. The triangles are TI values, whereas the solid line corresponds to the theoretical prediction (2.44).

Fig. (4) demonstrates that the reduced quantity

$$\frac{S(q,T)}{S(0,T)} = \frac{F(q\xi_{||})}{F(0)} = 4F(q\xi_{||}) \tag{2.39}$$

obtained in the continuum approximation gives an excellent description of the discrete (TI) results over many decades of the dimensionless variable $q\xi$; note that in the second equation we have made use of the property $F(0) = 1/4$.

The zero stress isothermal susceptibility is given by

$$\begin{aligned} \chi &= \lim_{h\to 0}\left(\frac{\partial\sigma}{\partial h}\right)_T \\ &= \beta D a^2 S(0,T) \\ &= \frac{1}{4\delta^2}\,|t|^{-4} \\ &= \left(\frac{1}{2\delta_c}\,\frac{T}{T_c}\right)^2 |t|^{-4} \quad , \end{aligned} \tag{2.40}$$

i.e. the corresponding critical exponent is $\gamma = 4$. Again with $\delta_c = 0.36$, Fig. (2) demonstrates excellent agreement of (2.40) with TI values over many decades.

At temperatures very near T_c and finite q, i.e. for $q\xi_{||} \gg 1$, $F(x) \sim 2/x^2$ and hence

$$S(q,T_c) \propto \frac{1}{(q\ell)^{2-\eta}} \tag{2.41}$$

with $\eta = 0$.

E. The DNA order parameter

The quantity which is directly accessible in DNA denaturation in the fraction of bound base pairs, which can be measured using UV absorbance. The probability $P(y < b, T)$ of finding a given base pair at an equilibrium distance smaller than b (equal to the fraction of bound pairs, with a proper choice of b), is given by

$$P_I(y < b, T) \;=\; \int_{-\infty}^{b} dy\; |\phi_0(y)|^2 \tag{2.42}$$

$$= 1 - \frac{\gamma(2\delta - 1, 2\delta e^{-ab})}{\Gamma(2\delta - 1)} \tag{2.43}$$

$$\approx (2\delta - 1)\ Ei(2\delta e^{-ab}) \tag{2.44}$$

where γ is the incomplete gamma function, Ei is the exponential-integral function, and the last line is valid in the vicinity of T_c. For the class of models effectively described by the Morse potential, the fraction of bound pairs approaches zero linearly as $T \to T_c$, for any value of b (cf. Fig.5). The slope, as expected, reflects the particular choice of b.

III. AN ALTERNATIVE VIEW OF THE TRANSITION: THERMAL STABILITY OF THE DOMAIN WALL

A. Elementary dynamics

The equation of motion corresponding to (2.1) is

$$m\ddot{y}_n = K(y_{n+1} + y_{n-1} - 2y_n) - \frac{\partial V}{\partial y_n} \tag{3.1}$$

or, in the continuum limit,

$$\ddot{y} = c_0^2 \frac{\partial^2 y}{\partial x^2} - \frac{1}{m}\frac{\partial V}{\partial y} \tag{3.2}$$

where $c_0 = \omega_0 \ell$. Relevant static configurations of the infinite chain with free ends, derivable from (3.2) are:
(a) The uniform solution at the minimum of $V(y)$, $y(x) \equiv 0$; this configuration corresponds to the absolute minimum of the total potential energy (equal to zero) and is stable with respect to small amplitude fluctuations; linearized solutions of (3.2) are optical phonons.
(b) For very large values of y, $V(y)$ is almost a constant; therefore, expressions which verify $d^2y/dx^2 = 0$, i.e. of the form $\lim_{M\to\infty}[y(x) - M] = C \cdot x$, where $C > 0$ is an arbitrary constant, are approximate solutions in the sense that they correspond to local minima of the total potential energy; linearization of (3.2) around them leads to an acoustic phonon spectrum.
(c) an exact, unbounded, domain-wall like solution

$$y_{DW}^{\pm}(x) = \frac{1}{a} \ln\left[1 + e^{\pm(x - x_0)/d}\right] \quad . \tag{3.3}$$

where $d = \ell/\sqrt{2R}$ and x_0 is an arbitrary constant.

The solution (3.3) is plotted in Fig. 6 for the case of the upper sign. It represents a nonlinear field configuration which "interpolates" from the stable minimum (a) to a particular member of the metastable configurations (b), with a slope $C = 1/(ad)$, and hence equal contributions to the elastic and the on-site potential energy densities (D per site). In other words it is a profile of a double chain where the two strands stick together if $x < x_0$, but strand separation grows linearly for all points $x \gg x_0$; the energy of the solution contains a term which is proportional to the number of sites to the right of x_0. More exactly, if lattice sites are numbered from 0 to N,

$$E_{DW}^{+} = \left(N - \frac{x_0}{\ell}\right) 2D + \mathcal{O}(N^0) \quad . \tag{3.4}$$

At zero temperature the profile (3.3) is not stable. Since

$$E_{DW}^{+}(x_0 \pm \ell) - E_{DW}^{+}(x_0) = \mp 2\ell D \tag{3.5}$$

the wall will spontaneously move to the right, "zipping" back the unbound portion of the double chain. We will consider below how this instability changes under the influence of temperature.

B. Linearisation around the DW

Consider small deviations with respect to (3.3), i.e.

$$y(x,t) = y_{DW}^{+}(x - x_0) + \sum_j \alpha_j f_j(x - x_0) e^{-i\omega_j t} \tag{3.6}$$

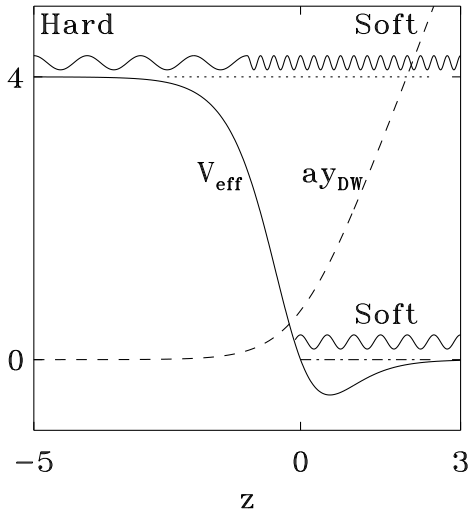

FIG. 6: The dashed line represents the domain wall solution (3.3) as a function of the dimensionless space variable z. The full line represents the effective potential of the Schrödinger-like equation (3.7). The potential marginally fails to support bound states. Scattering states with eigenvalues less than the top of the potential (i.e. between dashed and dashed-double-dotted lines) are confined to the right-half of the line (low-frequency acoustic phonons); those with higher eigenvalues consist of both transmitted and reflected waves with different wavevectors and hence different dispersion relations in the two halves of the line (corresponding to both hard, i.e. optical, and soft, i.e. acoustic phonons, cf. text).

where $|\alpha_j| \ll a$. The linearized eigenfunctions f_j satisfy the equation

$$-\frac{d^2 f_j}{dz^2} + 2\left[1 - \tanh z - \mathrm{sech}^2 z\right] f_j = \frac{2\omega_j^2}{R\omega_0^2} f_j \quad , \tag{3.7}$$

where $z = (x - x_0)/(2d)$. Eq. (3.7) is Schrödinger-like with an effective potential drawn in Fig. 6. It can be shown [19] that (3.7) has no bound states; scattering states are of two types:

(I) if $\omega_q^2 < 2R\omega_0^2$ they are confined to the right half of the z-axis; for $x \gg x_0$

$$f_q \sim \cos\left[k_- z + \delta_I\right] \equiv \cos\left[q(x - x_0) + \delta_I\right] \tag{3.8}$$

where

$$\frac{\delta_I}{2} = \arg\Gamma\left(ik_-\right) - \arg\Gamma\left(\frac{1}{2}\kappa_+ - 1 + \frac{i}{2}k_-\right) - \arg\Gamma\left(\frac{1}{2}\kappa_+ + 2 + \frac{i}{2}k_-\right) \tag{3.9}$$

$k_-^2 \equiv 2\omega_q^2/(R\omega_0^2)$, $\kappa^2 \equiv 4 - k_-^2$, $q \equiv k_-/(2d)$ and therefore

$$\frac{\omega_q}{\omega_0} = q\ell \quad \text{if } q\ell < \sqrt{2R} \tag{3.10}$$

i.e. the "phonons" with the low frequencies are soft, acoustic phonons, as one expects them to be, since they correspond to atoms oscillating on the flat portion of the Morse potential.

(II) in the high frequency case, i.e. if $\omega_q^2 > 2R\omega_0^2$, scattering states extend over the whole line and have both transmitted and reflected components. Specifically,

$$f_q(z) = \begin{cases} e^{-ik_- z} + \rho^{1/2} e^{i(k_- z + \delta_{II}^{\rho})} & \text{if } z \to \infty \\ \left(\frac{k_-}{k_+}\tau\right)^{1/2} e^{-i(k_+ z + \delta_{II}^{\tau})} & \text{if } z \to -\infty \end{cases} \tag{3.11}$$

where

$$\rho = \left[\frac{\sinh\frac{\pi}{2}\left(k_- - k_+\right)}{\sinh\frac{\pi}{2}\left(k_- + k_+\right)}\right]^2 \tag{3.12}$$

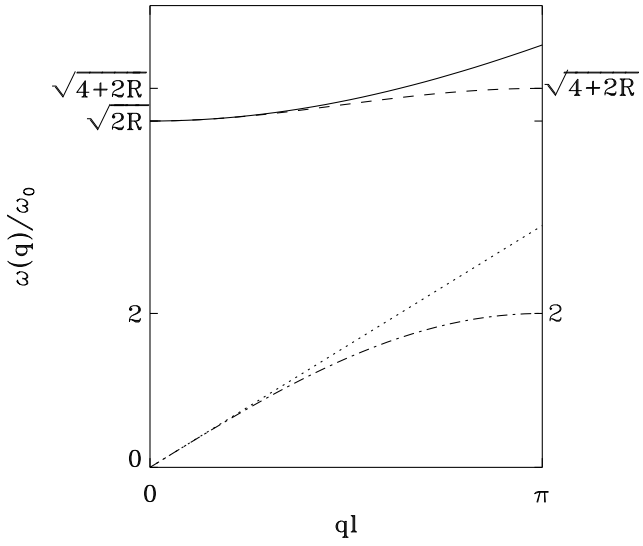

FIG. 7: Continuum limit dispersion relations for the soft (Eq. (3.10) as a dotted line) and hard (Eq. (3.13) as a solid line) phonons; they extend to $ql \to \infty$. The discrete dispersion relations (4.1) are also shown, with dashed line (hard) and dash-dotted line (soft). All curves have been drawn for $R = 10.1$; note the formation of a frequency gap between the two branches of the discrete spectrum for $R > 2$.

$\tau = 1 - \rho$, $k_+^2 = 4 - k_-^2$, $q_+ \equiv k_+/(2d)$ and therefore

$$\frac{\omega_q}{\omega_0} = \begin{cases} q\ell & \text{if } q\ell > \sqrt{2R},\ x \gg x_0 \\ \left[2R + (q_+\ell)^2\right]^{1/2} & \text{any } q_+,\ x \ll x_0 \end{cases} \tag{3.13}$$

i.e. the dispersion relation is different in the soft (unbound) segment and the hard (bound) segment of the line (see Fig. 7). Formally, we can combine the two results for the dispersion into two branches, one optical and one acoustic, for each value of q, without any restrictions. However, it should be borne in mind that the acoustic phonons physically reside in the soft (unbound) and the optical ones in the hard (bound) segment of the line.

For completeness we list the phase shifts

$$\delta_{II}^{\tau} = 2\arg\Gamma\left[2 + \frac{i}{2}(k_- + k_+)\right] - \arg\Gamma(1 + ik_+) - \arg\Gamma(1 + ik_-) - \pi \tag{3.14}$$

$$\delta_{II}^{\rho} = -2\arg\Gamma\left[2 + \frac{i}{2}(k_- + k_+)\right] - 2\arg\Gamma\left[2 + \frac{i}{2}(k_- - k_+)\right] + 2\arg\Gamma(1 + ik_-) \quad . \tag{3.15}$$

C. Free energy of the thermally dressed DW

At finite temperatures, the domain wall is accompanied by a phonon cloud. The phonon cloud contributes three terms to the free energy, which arise from cases I (soft), II (soft), II (hard) presented in the previous subsection. Because these phonons reside in different - and in general unequal - portions of the chain, their contributions to the free energy depend on the position of the DW. Specifically,

$$F_{soft} = k_B T \sum_q \ln \beta\hbar\omega_q^{ac} \tag{3.16}$$

$$F_{hard} = k_B T \sum_q \ln \beta\hbar\omega_q^{opt} \tag{3.17}$$

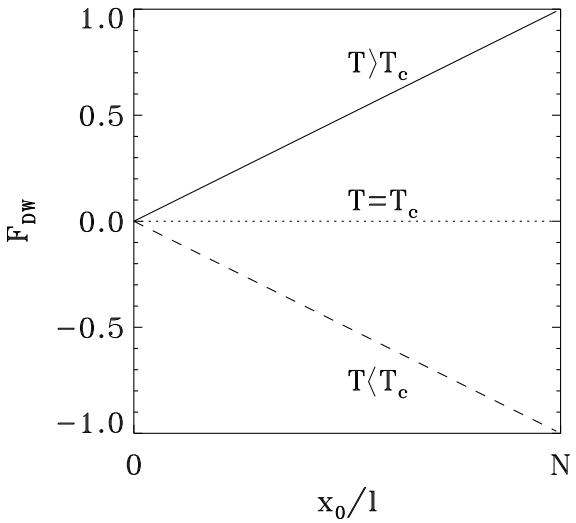

FIG. 8: Free energy of the DW (in units of D) for temperatures above ($T = 3/2T_c$, solid line), below ($T = 1/2T_c$, dashed line) and at T_c (dotted line), according to Eq. (3.21); the irrelevant constant has been omitted.

where contributions from soft modes have been combined. The sum over q can be replaced by a density of states determined by

$$q\,(N - x_0) \;=\; n\pi \quad , n = 0, 1, 2, ...(\text{soft}) \tag{3.18}$$
$$q\,(N + x_0) \;=\; n\pi \quad , n = 0, 1, 2, ...(\text{hard}) \quad . \tag{3.19}$$

This results in a phonon-cloud free energy

$$F_{phonon\ cloud} = k_B T x_0 \int_0^\infty \frac{dq}{\pi} \ln \frac{\omega_q^{opt}}{\omega_q^{ac}} + ... \tag{3.20}$$

where the ellipsis denotes terms independent of x_0 and, since the integrand is ultraviolet-convergent, we have extended the upper limit of the integration to infinity. This is consistent with the continuum limit treated in this work; an ultraviolet divergence present in the ellipsis can be corrected by the introduction of a lattice cutoff but this is irrelevant for the purposes of the present argument. Introducing the correct dispersion relations for optical and acoustic phonons, we can evaluate [14] the integral in (3.20). This results in a total free energy (DW plus phonon cloud)

$$F_{DW} = const + \left(k_B T \frac{\sqrt{2R}}{2} - 2D \right) \frac{x_0}{\ell} \quad . \tag{3.21}$$

Equation (3.21) is the central result of this section. It describes in very simple terms why and when the phase transition occurs. At temperatures lower than

$$T_c = \frac{2\sqrt{2}D}{k_B\sqrt{R}} = \frac{2\sqrt{2KD}}{ak_B} \tag{3.22}$$

the prefactor of x_0 is negative; the DW's natural tendency is towards high positive values of x_0, i.e. it "zips" the system back to the bound configuration. Conversely, at temperatures higher than T_c, thermal stability is achieved by a high negative value of x_0, i.e. the DW "opens up", unbinds the system. At the critical point, the DW is thermally (meta)stable at any position; this corresponds to physical realizations of the chain at criticality. It should be noted that the value of T_c predicted by the above DW argument coincides with the exact result (2.14) of the continuum limit. This supports the validity of the alternative description of the phase transition in terms of the thermal stability of the DW.

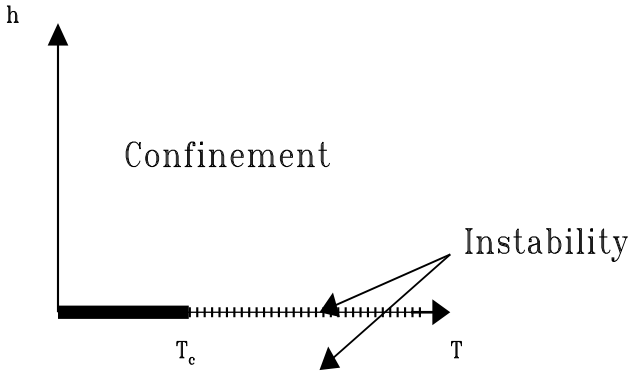

FIG. 9: Phase diagram in the (T, h) plane. At negative h, the system is unstable at all temperatures.

IV. DISCUSSION

We have given a detailed account of the exact thermodynamics and the scattering function $S(q, T)$ of a model used to describe thermal DNA denaturation, as well as other one-dimensional instabilities. The model deserves special attention for two reasons: (a) it is probably the simplest exactly solvable lattice model in one dimension which exhibits a true thermodynamic transition and satisfies all scaling laws (cf. below), and (b) the transition can be understood in terms of the thermal stability of a soliton-like nonlinear configuration. A number of comments are in order:

1. None of the "prohibitions" of phase transitions in one dimension apply to this model. The theorem by Gursey [15] and the van-Hove demonstration [16], extended by Ruelle [17] apply to systems with pair interactions only. The standard Landau [6] argument, which covers systems with on-site potentials (e.g. ϕ^4) rests on the finiteness of the DW energy.

2. The critical exponents calculated analytically from the properties of the Schrödinger equation (2.10) satisfy all applicable scaling laws, i.e $d\nu_{||} = 2 - \alpha = \gamma + 2\beta$ and $\gamma = (2 - \eta)\nu_{||}$. Figs. 2-4 demonstrate very good agreement between the thermodynamic behavior calculated from numerical TI, and the one obtained exactly from Eq. (2.10). It appears that "universality" extends to prefactors and not just to exponents - provided that corrections due to the absolute value of critical point are taken into account. This in spite of the fact that the TI values refer to a system with a very high degree of discreteness ($R = 10.1$).

3. It is instructive to view the phase diagram in the (h, T) plane (Fig. 9). For positive values of the external field h, there is confinement at all temperatures. In the limit $h \to 0^+$, the system approaches a confined ($T < T_c$), or a deconfined ($T > T_c$) state. The TI (and the exact, Schrödinger) solutions presented here refer to the limit of the $(h = 0^+, T)$ confined state as $T \to T_c^-$ (thick line). Finally, at any $h < 0$, the system is unstable.

4. The scattering function (2.37) shows typical Ornstein-Zernike behavior. Its form demands that at least some of the weight cannot come from phonons. We will report details of critical dynamics in a separate paper. Preliminary results suggest the occurrence of a central peak. It will be interesting to relate critical dynamics with large-scale fluctuations of nonlinear configurations.

5. The estimate (3.22) of the critical temperature can be extended to cover discrete systems. This is done by introducing the discrete dispersion relations

$$\frac{\omega_q^2}{\omega_0^2} = \begin{cases} 2\left(1 - \cos(q\ell)\right) + 2R & \text{(optical)} \\ 2\left(1 - \cos(q\ell)\right) & \text{(acoustic)} \end{cases} \tag{4.1}$$

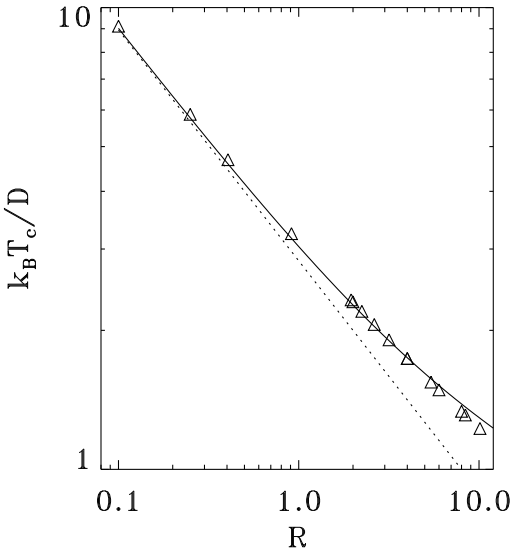

FIG. 10: Dependence of the critical temperature on the discreteness parameter R. The dotted curve shows the continuum estimate, (3.22). The solid curve corresponds to (4.4), whereas the triangles denote the numerical TI values; agreement is excellent for values of R well into the discrete regime; nonetheless, systematic deviations can be seen, starting at $R > 4$ (cf. text).

in Eq. (3.20) which describes the free energy of the phonon cloud accompanying the DW. Numerical experiments have demonstrated [20] that the asymptotic slope of the DW is given by the same function of R for arbitrary levels of discreteness, i.e. $\lim_{n\to\infty}(y_n - y_{n-1})/\ell = 1/(ad) = \sqrt{2R}/(a\ell) = \sqrt{2D/K}/\ell$. It follows that each site which finds itself in the high temperature phase contributes an elastic energy equal to $(1/2)K(y_n - y_{n-1})^2 = D$ and an on-site energy equal to D, i.e. a total of $2D$. This is a property of the DW, continuum or discrete. Therefore, the only modification to (3.21) and (3.22) comes from the entropy of the phonon cloud. In detail, using [14]

$$I^*(R) \equiv \frac{1}{2\pi}\int_0^\pi dx \ln[1 - \cos x + R] = \ln\left[\frac{\sqrt{R} + \sqrt{R+2}}{2}\right] \tag{4.2}$$

we obtain from (3.20)

$$F_{phonon\ cloud} = \frac{k_B T x_0}{\ell}\left[I^*(R) - I^*(0)\right] \tag{4.3}$$

which results in the estimate

$$T_c = \frac{2D}{k_B \ln\left[\sqrt{R/2} + \sqrt{1 + R/2}\right]} \quad . \tag{4.4}$$

In the limit $R \ll 1$, Eq. (4.4) reduces to Eq. (3.22). It can be seen in Fig. (10) that the *nonperturbative* theoretical estimate (4.4) is in excellent agreement with TI numerical results even for values of R well into the discrete regime, $R \gg 1$. Systematic discrepancies appear at values of $R > 4$ and seem to grow as R increases further. The origin of these discrepancies is currently under investigation; preliminary numerical results [20] suggest a significant complexity in the properties of the DW at values of $R > 4$.

Within the scope of the present work, we feel it is justified to state that (a) in the continuum approximation, and (b) even at moderate levels of discreteness, our understanding of a prototype one-dimensional phase transition can be considerably enhanced by making use of the concept of the thermal stability of a distinctly nonlinear entity. In more plain terms: formation of the DW can be thought of as "driving" the thermodynamic instability.

Acknowledgments

We thank P. C. W. Holdsworth and D. Mukamel for helpful discussions. This work has been partially supported by EU contract No. HPRN-CT-1999-00163 (LOCNET network).

---

[1] J. A. Krumhansl and J. R. Schrieffer, Phys. Rev. B **11**, 3535 (1975).
[2] M. Peyrard and A.R. Bishop, Phys. Rev. Lett. **62**, 2755 (1989).
[3] T. Dauxois, M. Peyrard and A. R. Bishop, Phys. Rev. E **47**, R4 (1993).
[4] T. Dauxois and M. Peyrard, Phys. Rev. E **51**, 4027 (1995).
[5] D. M. Kroll and R. Lipowski, Phys. Rev. B **28**, 5273 (1983); R. Lipowski, Phys. Rev. B **32**, 1731 (1985).
[6] L. D. Landau and E. M. Lifshitz, *Statistical Physics*, Pergamon Press (1980).
[7] A very concise summary of exact results has been reported by N. Theodorakopoulos, T. Dauxois and M. Peyrard, Phys. Rev. Lett. **85**, 6 (2000).
[8] M. Kac, G. E. Uhlenbeck and P. C. Hemmer, J. Math. Phys. **4**, 216 (1963).
[9] Y-L Zhang, W-M Zheng, J-X Liu, Y. Z. Chen, Physical Review E **56**, 7100 (1997).
[10] R. A. Guyer and M. D. Miller, Phys. Rev. A **17**, 1205 (1978).
[11] P. M. Morse and E. C. G. Stueckelberg, Phys. Rev. **33**, 932 (1929).
[12] M. Martin Nieto and L. M. Simmons Jr, Phys. Rev. A **19**, 438 (1979).
[13] M. Abramowitz and I. A. Stegun, *Handbook of Mathematical Functions*, Dover (1965)
[14] I. S. Gradshtein and I. M. Ryzhik, *Tables of Integrals, Series, and Products*, Academic Press (1994).
[15] F. Gursey, Proc. Cambridge Phil. Soc. **46**, 182 (1950).
[16] L. van Hove, Physica **16**, 137 (1950).
[17] D. Ruelle, Commun. Math. Phys. **9**, 267 (1968)
[18] W.F. Buell and B.A. Shadwick, Am. J. Phys. **63**, 256-258 (1995)
[19] P.M. Morse and H. Feshbach, *Methods of theoretical physics.* McGraw-Hill, N.Y. (1953), Chap. 12.
[20] M. Peyrard, T. Dauxois, N. Theodorakopoulos (unpublished)